A Neural-Network-Based Space-Vector PWM Controller for Voltage-Fed Inverter Induction Motor Drive

Joao O. P. Pinto, *Student Member, IEEE*, Bimal K. Bose, *Life Fellow, IEEE*, Luiz Eduardo Borges da Silva, *Member, IEEE*, and Marian P. Kazmierkowski, *Fellow, IEEE*

***Abstract*—A neural-network-based implementation of space-vector modulation (SVM) of a voltage-fed inverter has been proposed in this paper that fully covers the undermodulation and overmodulation regions linearly extending operation smoothly up to square wave. A neural network has the advantage of very fast implementation of an SVM algorithm that can increase the converter switching frequency, particularly when a dedicated application-specific integrated circuit chip is used in the modulator. The scheme has been fully implemented and extensively evaluated in a V/Hz-controlled 5-hp 60-Hz 230-V induction motor drive. The performances of the drive with artificial-neural-network-based SVM are excellent. The scheme can be easily extended to a vector-controlled drive.**

***Index Terms*—Drive, induction motor, neural network, pulsewidth modulation.**

I. Introduction

SPACE-VECTOR modulation (SVM) has recently grown as a very popular pulsewidth modulation (PWM) method for voltage-fed converter ac drives because of its superior harmonic quality and extended linear range of operation [1]. However, a difficulty of SVM is that it requires complex online computation that usually limits its operation up to several kilohertz of switching frequency. Of course, switching frequency can be extended by using a high-speed digital signal processor (DSP) and simplifying computations with the help of lookup tables. Lookup tables, unless very large, tend to reduce the pulsewidth resolution. Very recently, a novel decision-tree-based SVM technique has been proposed [2] which extends the switching frequency up to 16 kHz in a low-inductance servo motor drive. Power semiconductor switching speed has improved dramatically in recent years. Modern ultrafast insulated gate bipolar transistors (IGBTs) demand switching frequency as high as 50 kHz. The DSP-based SVM practically fails in this region where artificial-neural-network (ANN)-based SVM can possibly take over.

The application of ANNs is recently growing in power electronic systems. A feedforward ANN implements nonlinear input–output mapping. The computational delay of this mapping becomes negligible if parallel architecture of the network is implemented by an application-specific integrated circuit (ASIC) chip. A feedforward carrier-based PWM technique, such as SVM, can also be looked upon as a nonlinear mapping phenomenon where the command phase voltages are sampled at the input and the corresponding pulsewidth patterns are established at the output. Therefore, it appears logical that a backpropagation-type ANN which has high computational capability can implement an SVM algorithm. The ANN can be conveniently trained offline with the data generated by calculation of the SVM algorithm. Note that the ANN has inherent learning capability that can give improved precision by interpolation unlike the standard lookup table method.

In the past, a neural network was generally considered for implementation of instantaneous current control PWM [4]–[7] where the sinusoidal phase current commands were compared with the respective feedback currents, and the resulting loop errors generated the pulsewidth signals through a feedforward ANN. Current control PWM does not give optimum performance. Besides, it cannot be used in voltage control PWM in drives which are so widely used in industry. The ANN-based SVM of a voltage-fed inverter was first proposed in [8], where the authors considered the undermodulation region only. They suggested the use of competitive neural network architecture to identify the inverter switching states and the corresponding voltage magnitudes for the impressed command voltage.

This paper describes feedforward ANN-based SVM that fully covers the undermodulation and overmodulation regions extending operation up to square wave. In the beginning, the SVM theory has been briefly reviewed with mathematical analysis for the overmodulation range. Then, equations for algorithms of undermodulation and overmodulation (Mode-1 and Mode-2) have been developed in detail and simplified so that the undermodulation algorithm can be extended in the overmodulation range by modification of a voltage scale factor. A backpropagation-type feedforward ANN is trained offline

Paper IPCSD 00–036, presented at the 1999 Industry Applications Society Annual Meeting, Phoenix, AZ, October 3–7, and approved for publication in the IEEE TRANSACTIONS ON INDUSTRY APPLICATIONS by the Industrial Drives Committee of the IEEE Industry Applications Society. Manuscript submitted for review October 15, 1999 and released for publication July 17, 2000. This work was supported in part by the U.S.–Poland MSC Joint Fund II of Poland and CAPES of Brazil.

J. O. P. Pinto and B. K. Bose are with the Department of Electrical Engineering, University of Tennessee, Knoxville, TN 37996-2100 USA (e-mail: jpinto@utk.edu; bbose@utk.edu).

L. E. Borges is with the Department of Electrical Engineering, University of Tennessee, Knoxville, TN 37996-2100 USA, on leave from the Escola Federal de Engenharia de Itajubá, Itajubá 37500-000, Brazil (e-mail: leborges@iee.efei.rmg.br).

M. P. Kazmierkowski is with the Institute of Control and Industrial Electronics, Warsaw University of Technology, Warsaw 00-662, Poland (e-mail: kazmierkowski@isep.pw.edu.pl).

Publisher Item Identifier S 0093-9994(00)10421-9.

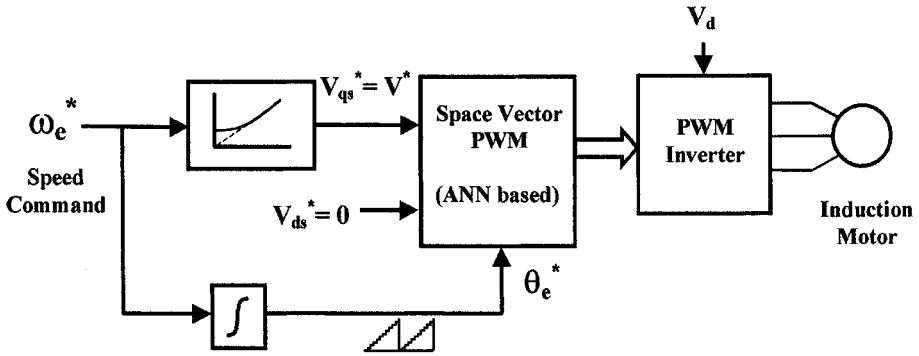

Fig. 1. V/Hz control of induction motor showing neural-network-based implementation.

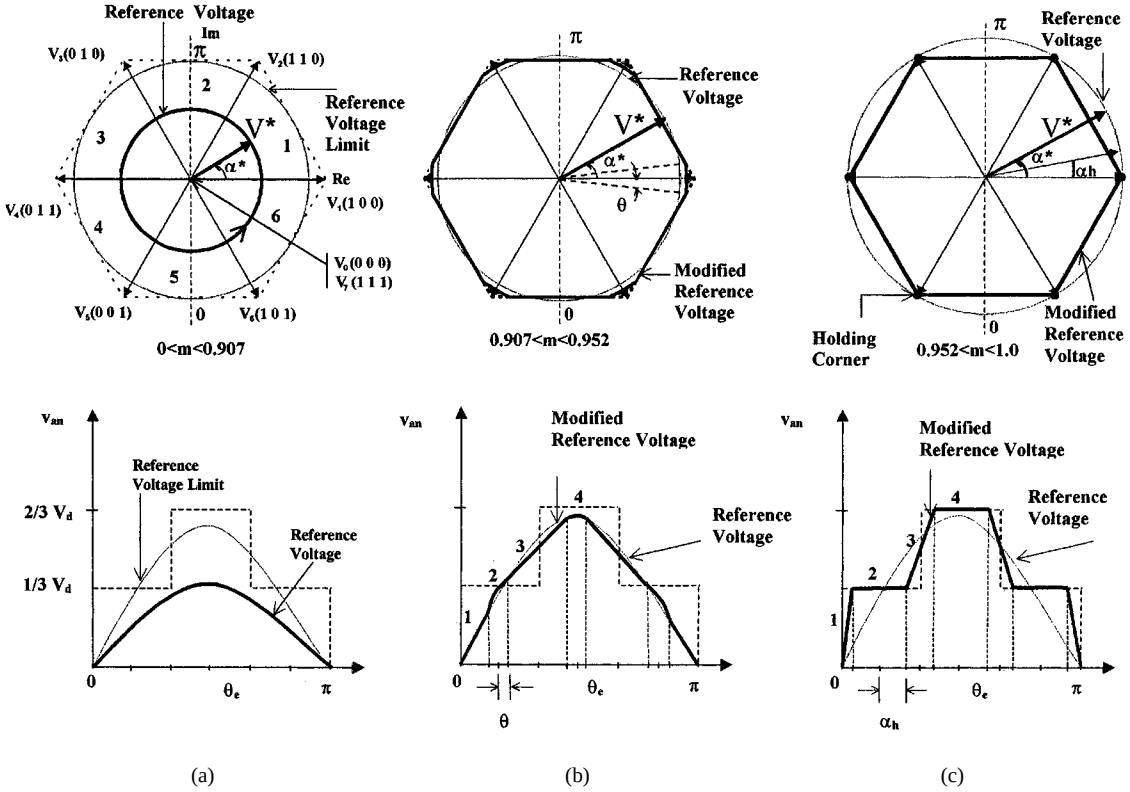

Fig. 2. Voltage trajectories in undermodulation and overmodulation regions and the corresponding phase voltages. (a) Undermodulation. (b) Overmodulation Mode-1. (c) Overmodulation Mode-2.

with the data generated by this simple algorithm, and then extensively evaluated on a V/Hz-controlled induction motor drive.

II. Space-Vector PWM in Undermodulation and Overmodulation Regions

The SVM theory, in general, has been well discussed in the literature, and a number of authors [1], [10]–[13] have described its operation in the overmodulation region. The principles are briefly reviewed here, adding analysis in the overmodulation region with the goal of its ANN implementation. The principles described in [10] will be generally accepted. Fig. 1 shows the block diagram of an open-loop V/Hz-controlled induction motor drive incorporating the proposed ANN-based SVM controller. The command voltage $V_{qs}^*(=V^*)$ is generated from the frequency or speed command, and the angle command θ_e^* is obtained by integrating the frequency, as shown. The output of the modulator generates the PWM patterns for the inverter switches. For a vector-controlled drive with synchronous current control, both V_{qs}^* and V_{ds}^* signals are present and, therefore, the SVM controller input signals can be modified as follows:

$$V^* = \sqrt{V_{qs}^2 + V_{ds}^2} \tag{1}$$

$$\theta_e^{*'} = \theta_e^* + \tan^{-1}(V_{qs}/V_{ds}). \tag{2}$$

Fig. 2 explains SVM operation in the undermodulation and overmodulation regions, and the corresponding line-to-neutral average phase voltage (v_{an}) waves are shown in the lower part. It is well known that the operation of a three-phase two-level voltage-fed inverter is characterized by eight switching states of which six [$V_1(100) - V_6(101)$] are active to form a hexagon, and two [$V_0(000)$ and $V_7(111)$] are zero states that lie at the

origin. The operation in undermodulation and overmodulation is determined by the modulation factor m which is defined as

$$m = \frac{V^*}{V_{1sw}} \tag{3}$$

where V^* is the magnitude of command or reference voltage vector and V_{1sw} is the peak value ($2V_d/\pi$) of square (or six step) voltage wave. The modulation factor varies between 0–1.

A. Undermodulation ($0 < m < 0.907$)

In the undermodulation or linear region, shown in Fig. 2(a), the rotating reference voltage V^* remains within the hexagon. The mode ends at the upper limit when V^* describes the inscribed circle at $m = 0.907$. The SVM strategy in this region is based on generating three consecutive switching voltage vectors in a sampling period (T_s) such that the average output voltage matches with the reference voltage. The equations for effective time of the inverter switching states can be given as

$$t_a = 2 \cdot K \cdot V^* \sin(\pi/3 - \alpha^*) \tag{4}$$

$$t_b = 2 \cdot K \cdot V^* \sin \alpha^* \tag{5}$$

$$t_0 = \frac{T_s}{2} - (t_a + t_b) \tag{6}$$

where

- t_a time of switching vector that lags V^*;
- t_b time of switching vector that leads V^*;
- t_0 time of zero-switching vector;
- T_s $= 1/f_s$, sampling time (f_s = switching frequency);
- α^* angle of V^* in a 60° sector;
- K $= (\sqrt{3}T_s)/(4 \cdot V_d)$.

The times are distributed to generate symmetrical PWM pulses (see Fig. 6).

B. Overmodulation Mode-1 ($0.907 < m < 0.952$)

The overmodulation or nonlinear operation starts when the reference voltage V^* exceeds the hexagon boundary. In overmodulation Mode-1, shown in Fig. 2(b), V^* crosses the hexagon at two points in each sector. To compensate loss of fundamental voltage, i.e., to track with the reference voltage, a modified reference voltage trajectory is selected that remains partly on the hexagon and partly on a circle. The circular part of the trajectory has extended radius $V_m^*(V_m^* > V^*)$ and crosses the hexagon at angle θ, as shown in the figure. Note that (4)–(6) remain valid for the circular part of the trajectory (except V^* is replaced by V_m). However, on the hexagon trajectory, time t_0 vanishes, giving t_a and t_b expressions as

$$t_a = \frac{T_s}{2}\left(\frac{\sqrt{3}\cos\alpha^* - \sin\alpha^*}{\sqrt{3}\cos\alpha^* + \sin\alpha^*}\right) \tag{7}$$

$$t_b = \frac{T_s}{2} - t_a. \tag{8}$$

The v_{an} voltage wave is given by approximate linear segments for the hexagon trajectory and sinusoidal segments for the circular trajectory, as shown in the lower part of Fig. 2(b). The equations for the four voltage segments in the first quarter-cycle [12] can be given as

segment 1:

$$v_1 = m_1 \cdot \theta_e, \qquad 0 < \theta_e < \frac{\pi}{6} - \theta \tag{9}$$

segment 2:

$$v_2 = V_m^* \cdot \sin\theta_e, \qquad \frac{\pi}{6} - \theta < \theta_e < \frac{\pi}{6} + \theta \tag{10}$$

segment 3:

$$v_3 = A + \frac{m_1}{2} \cdot \theta_e, \qquad \frac{\pi}{6} + \theta < \theta_e < \frac{\pi}{2} - \theta \tag{11}$$

segment 4:

$$v_4 = V_m^* \cdot \sin\theta_e, \qquad \frac{\pi}{2} - \theta < \theta_e < \frac{\pi}{2} \tag{12}$$

where $\theta_e = \omega_e t$, $m_1 = 2V_d/\pi$ is the slope of linear segment 1, $A = V_d/6$, and V_m^* is the modified reference voltage. The voltage V_m^* can be defined as a function of crossover angle θ by equating (9) and (10) at angle $(\pi/6 - \theta)$ as

$$V_m^* = \frac{2 \cdot V_d(\pi/6 - \theta)}{\pi \cdot \sin(\pi/6 - \theta)}. \tag{13}$$

Because of quarter-cycle symmetry, the fundamental output voltage (V_1) expression can be written from (9) to (12) as

$$V_1 = \frac{4}{\pi}\left[\int_0^{\pi/6-\theta} v_1 \sin\theta_e \, d\theta_e + \int_{\pi/6-\theta}^{\pi/6+\theta} v_2 \sin\theta_e \, d\theta_e + \int_{\pi/6+\theta}^{\pi/2-\theta} v_3 \sin\theta_e \, d\theta_e + \int_{\pi/2-\theta}^{\pi/2} v_4 \sin\theta_e \, d\theta_e\right]. \tag{14}$$

A computer program is written to solve crossover angle θ as a function of modulation factor m from (3) and (9) to (14). Fig. 3(a) shows the plot of this relation. Mode-1 ends when angle $\theta = 0$ at $m = 0.952$, i.e., the trajectory is on the hexagon giving only linear segments of the v_{an} voltage wave.

C. Overmodulation Mode-2 ($0.952 < m < 1.0$)

In overmodulation Mode-2, the reference vector V^* increases further. Therefore, the actual trajectory is modified so that the output fundamental voltage matches that of the reference voltage, as discussed previously. The operation in this region, as explained in Fig. 2(c), is characterized by partly holding the modified vector at the hexagon corner for holding angle α_h, and partly tracking the hexagon sides in every sector. During holding angle, the magnitude of v_{an} remains constant, whereas during hexagon tracking, the voltage changes almost linearly, as shown in the lower part of Fig. 2(c). At the end of Mode-2, the linear segments vanish, giving six-step or square-wave operation when the modified vector is held at hexagon corners for 60°, i.e., $\alpha_h = 30°$. An expression for modified α^* angle (α_m^*) in Mode-2 can be given as [10]

$$\alpha_m^* = \begin{cases} 0, & 0 < \alpha^* < \alpha_h \\ \dfrac{\alpha^* - \alpha_h}{\pi/6 - \alpha_h} \cdot \dfrac{\pi}{6}, & \alpha_h < \alpha^* < \pi/3 - \alpha_h \\ \dfrac{\pi}{3}, & \pi/3 - \alpha_h < \alpha^* < \pi/3. \end{cases} \tag{15}$$

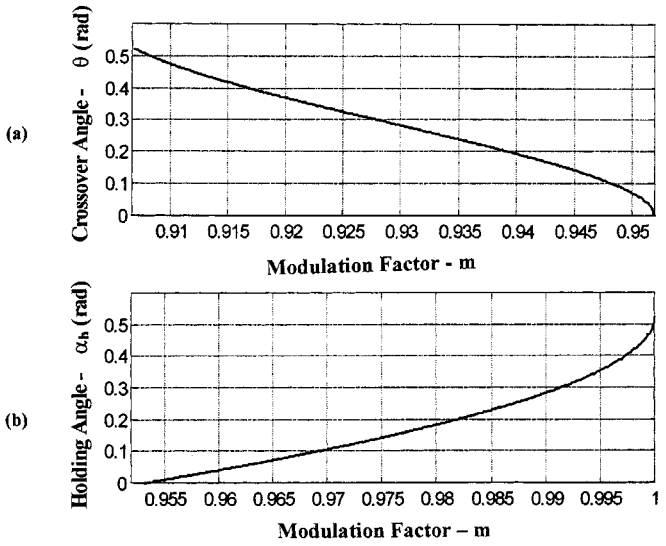

Fig. 3. (a) Modulation factor (m) relation with crossover phase angle (θ) in overmodulation Mode-1. (b) Modulation factor (m) relation with holding angle (α_h) in overmodulation Mode-2.

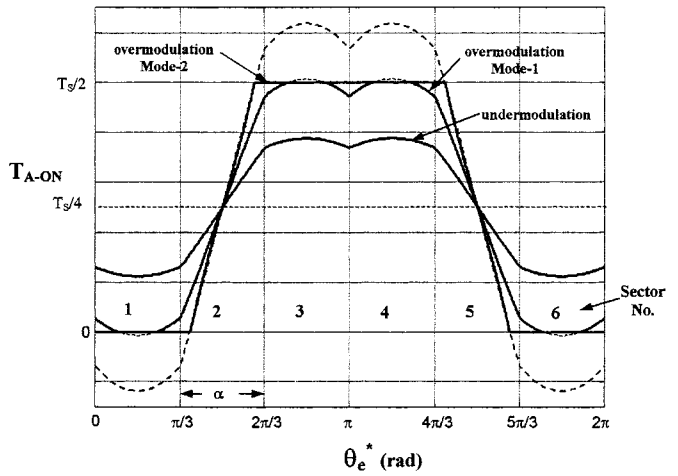

Fig. 4. Turn-on time ($T_{A-\mathrm{ON}}$) of phase A as function of angle θ_e in different sectors.

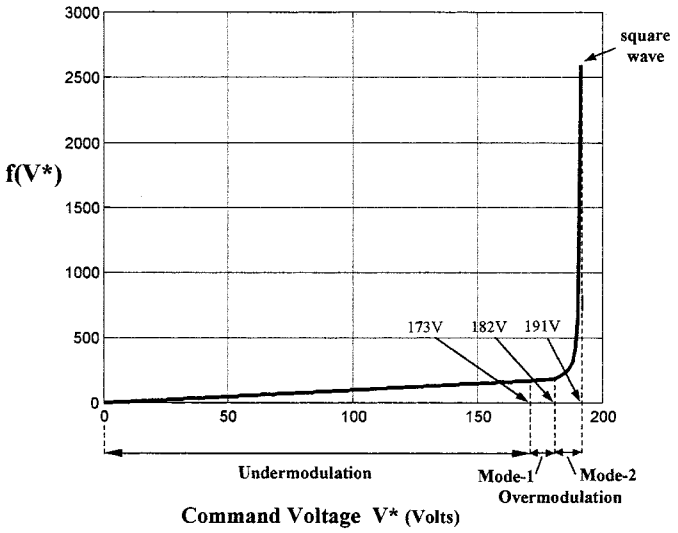

Fig. 5. $f(V^*) - V^*$ relation in undermodulation and overmodulation regions.

For the phase voltage (v_{an}) wave, the equations for the four segments in the first quarter-cycle [12] can be given as

segment 1:

$$v_1 = m_1' \cdot \theta_e, \qquad 0 < \theta_e < \frac{\pi}{6} - \alpha_h \tag{16}$$

segment 2:

$$v_2 = \frac{V_d}{3}, \qquad \frac{\pi}{6} - \alpha_h < \theta_e < \frac{\pi}{6} + \alpha_h \tag{17}$$

segment 3:

$$v_3 = A' + m_2 \cdot \theta_e, \qquad \frac{\pi}{6} + \alpha_h < \theta_e < \frac{\pi}{2} - \alpha_h \tag{18}$$

segment 4:

$$v_4 = \frac{2 \cdot V_d}{3}, \qquad \frac{\pi}{2} - \alpha_h < \theta_e < \frac{\pi}{2} \tag{19}$$

where

$$m_1' = \frac{V_d}{3(\pi/6 - \alpha_h)}$$
$$m_2 = \frac{V_d}{3(\pi/3 - 2\alpha_h)}$$
$$A' = \frac{V_d(\pi/6 - 3\alpha_h)}{3(\pi/3 - 2\alpha_h)}.$$

Again, because of quarter-cycle symmetry, the fundamental voltage V_1 expression can be given as

$$V_1 = \frac{4}{\pi}\left[\int_0^{\pi/6-\alpha_h} v_1 \sin\theta_e \, d\theta_e + \int_{\pi/6-\alpha_h}^{\pi/6+\alpha_h} v_2 \sin\theta_e \, d\theta_e + \int_{\pi/6+\alpha_h}^{\pi/2-\alpha_h} v_3 \sin\theta_e \, d\theta_e + \int_{\pi/2-\alpha_h}^{\pi/2} v_4 \sin\theta_e \, d\theta_e\right]. \tag{20}$$

For the output fundamental voltage to match with the reference voltage, a relation between holding angle α_h and modulation factor m can be derived from (3) and (16) to (20). The relation is plotted in Fig. 3(b).

III. Neural-Network-Based Space-Vector PWM

The SVM algorithm described in the previous section will be utilized to generate training data for ANN-based SVM. In the timer-based method, discussed in this section, the algorithm will be somewhat modified and then simplified.

A. Undermodulation Region

Consider typical undermodulation PWM waveforms shown in Fig. 6 which are drawn for sector $S = 1$ of Fig. 2(a). For any α^* angle, the timing intervals t_a, t_b, and t_0 are given by (4)–(6), respectively. Similar timing intervals can be calculated for all

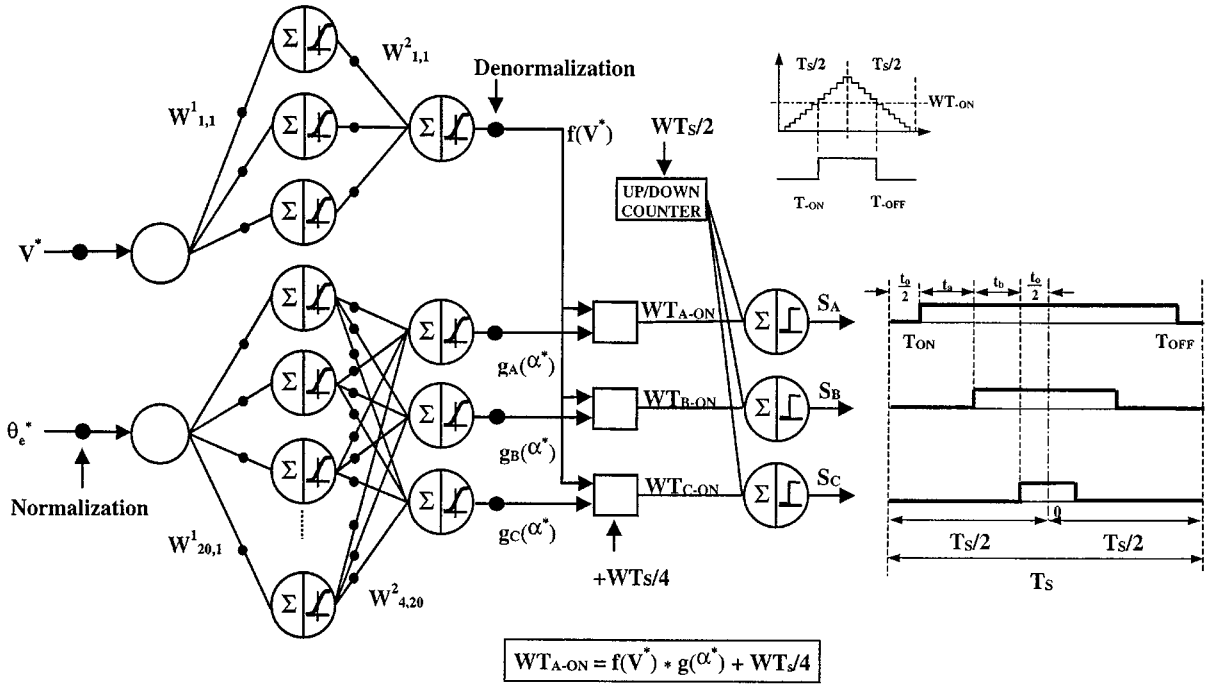

Fig. 6. Neural network topology (2-20-4) for PWM wave synthesis.

six sectors and, correspondingly, the phase *A* turn-on time can be expressed as

$$T_{A-\mathrm{ON}} = \begin{cases} \dfrac{t_0}{2} = \dfrac{T_s}{4} + K\cdot V^*\left[-\sin\left(\dfrac{\pi}{3}-\alpha^*\right)-\sin(\alpha^*)\right], & S=1,6 \\ \dfrac{t_0}{2}+t_b = \dfrac{T_s}{4} + K\cdot V^*\left[-\sin\left(\dfrac{\pi}{3}-\alpha^*\right)+\sin(\alpha^*)\right], & S=2 \\ \dfrac{t_0}{2}+t_a+t_b = \dfrac{T_s}{4} + K\cdot V^*\left[\sin\left(\dfrac{\pi}{3}-\alpha^*\right)+\sin(\alpha^*)\right], & S=3,4 \\ \dfrac{t_0}{2}+t_a = \dfrac{T_s}{4} + K\cdot V^*\left[\sin\left(\dfrac{\pi}{3}-\alpha^*\right)-\sin(\alpha^*)\right], & S=2. \end{cases} \tag{21}$$

Because of symmetry, the corresponding turn-off time is given as

$$T_{A-\mathrm{OFF}} = T_s - T_{A-\mathrm{ON}}. \tag{22}$$

Equation (21) can be written in the general form

$$T_{A-\mathrm{ON}} = T_s/4 + f(V^*)\cdot g(\alpha^*) \tag{23}$$

where $f(V^*)$ is the voltage amplitude scale factor and

$$g(\alpha^*) = \begin{cases} K\left[-\sin\left(\dfrac{\pi}{3}-\alpha^*\right)-\sin(\alpha^*)\right], & S=1,6 \\ K\left[-\sin\left(\dfrac{\pi}{3}-\alpha^*\right)+\sin(\alpha^*)\right], & S=2 \\ K\left[\sin\left(\dfrac{\pi}{3}-\alpha^*\right)+\sin(\alpha^*)\right], & S=3,4 \\ K\left[\sin\left(\dfrac{\pi}{3}-\alpha^*\right)-\sin(\alpha^*)\right], & S=5 \end{cases} \tag{24}$$

which is defined as turn-on pulsewidth function at unit amplitude ($f(V^*) = 1$). In the undermodulation region, the scale factor is linear, i.e., $f(V^*) = V^*$ (see Fig. 5). Equation (24) is plotted for all sectors in Fig. 4. For phases *B* and *C*, the $T_{A-\mathrm{ON}}$ curves are similar but respectively phase shifted by 120°. At the upper limit of undermodulation, the curve will reach the clamping levels $T_s/2$ and 0, as indicated in the figure. At the lower limit, $V^* = 0$ which makes $T_{A-\mathrm{ON}}$ always equal to $T_s/4$.

B. Overmodulation Mode-1

As discussed before, the modified voltage trajectory in Mode-1 is characterized by a part on the hexagon and a part on a circle. The circular part of the trajectory gives $T_{A-\mathrm{ON}}$ the same as (24) except $f(V^*) = V_m^*$ which is given by (13). Note that the scale factor is a nonlinear function of θ angle, i.e., modulation factor m. On the hexagon trajectory, $T_{A-\mathrm{ON}}$ for the different sectors can be calculated as

$$T_{A-\mathrm{ON}} = \begin{cases} \dfrac{t_0}{2} = 0, & S=1,6 \\ \dfrac{t_0}{2}+t_b = \dfrac{T_s}{2} - \dfrac{T_s}{2}\left(\dfrac{\sqrt{3}\cdot\cos\alpha^* - \sin\alpha^*}{\sqrt{3}\cdot\cos\alpha^* + \sin\alpha^*}\right), & S=2 \\ \dfrac{t_0}{2}+t_a+t_b = \dfrac{T_s}{2}, & S=3,4 \\ \dfrac{t_0}{2}+t_a = \dfrac{T_s}{2} - \dfrac{T_s}{2}\left(\dfrac{\sqrt{3}\cdot\cos\alpha^* - \sin\alpha^*}{\sqrt{3}\cdot\cos\alpha^* + \sin\alpha^*}\right), & S=5 \end{cases} \tag{25}$$

where t_a and t_b expressions are given by (7) and (8), respectively. The typical time $T_{A-\mathrm{ON}}$ is plotted in Fig. 4 for all the

TABLE I
DRIVE SYSTEM PARAMETERS

DC-link voltage (V_d)	300 V
Sampling time (T_s)	50 μs (and 100 μs)
Induction motor	5 hp 230 V four pole, Reliance Electric NEMA-Class B Frequency range: 0–60 Hz Power factor (full load): 0.85 Efficiency (full load): 86% Stator resistance (R_s): 0.5814 Ω Rotor resistance (R_r): 0.4165 Ω Stator leakage inductance (L_{ls}): 3.479 mH Rotor leakage inductance (L_{lr}): 4.15 mH Magnetizing inductance (L_m): 78.25 mH Rotor inertia (J): 0.1 kg·m^2 Fan load ($T_L = K\omega_r^2$): $K = 8.25 \times 10^5$

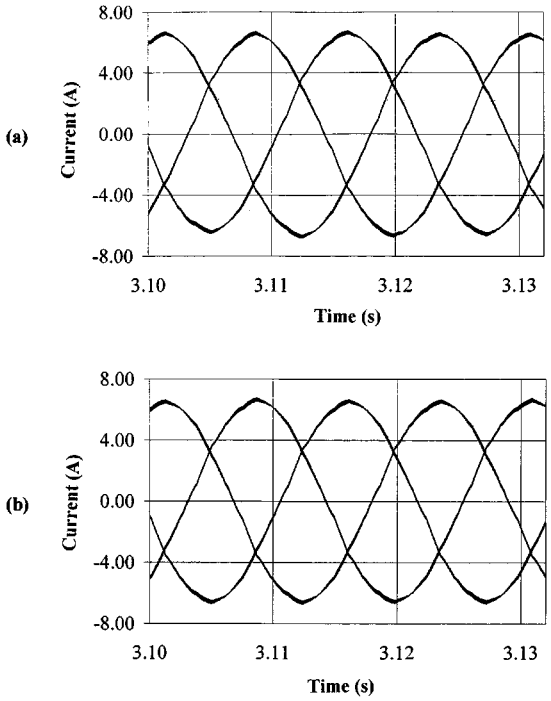

Fig. 7. Undermodulation phase current waves at 45 Hz. (a) Neural-network-based SVM. (b) Conventional DSP-based SVM.

sectors which indicates clamping at 0 and $T_s/2$. Note that, as the modulation factor m increases, the angle θ decreases and the greater amount of the trajectory remains on the hexagon. This increases the clamping regions in sectors $S = 1$, 3, 4, and 6, and steepens the slope of the nearly straightline segments in $S = 2$ and 5. At the end of Mode-1 that corresponds to fully hexagon trajectory, the sectors 1, 3, 4, and 6 remain fully clamped.

C. Overmodulation Mode-2

The time $T_{A-\mathrm{ON}}$ expression in Mode-2 is given by (25), except the angle α^* is replaced by α_m^* which is given by (15).

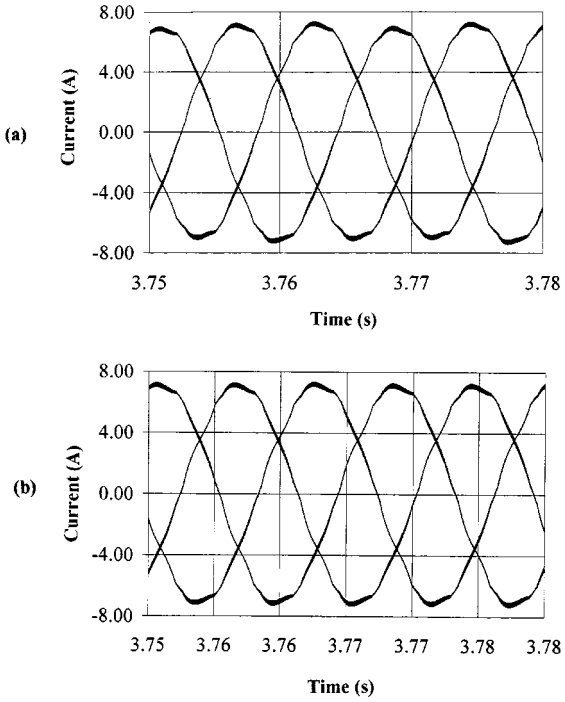

Fig. 8. Overmodulation Mode-1 phase current waves at 56 Hz. (a) Neural-network-based SVM. (b) Conventional DSP-based SVM.

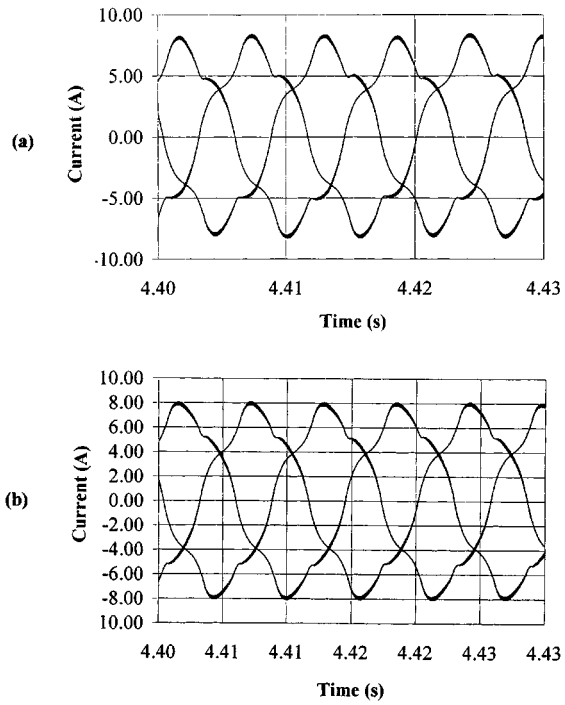

Fig. 9. Overmodulation Mode-2 phase current waves at 59 Hz. (a) Neural-network-based SVM. (b) Conventional DSP-based SVM.

The plot of the $T_{A-\mathrm{ON}}$ curve in Fig. 4 indicates full clamping in sectors 1, 3, 4, and 6 and partial clamping in sectors 2 and 5. At the end of Mode-2, clamping occurs in all the sectors and the $T_{A-\mathrm{ON}}$ curve is given by a square wave clamped at the levels $T_s/2$ and 0. This describes the square-wave operation of the inverter.

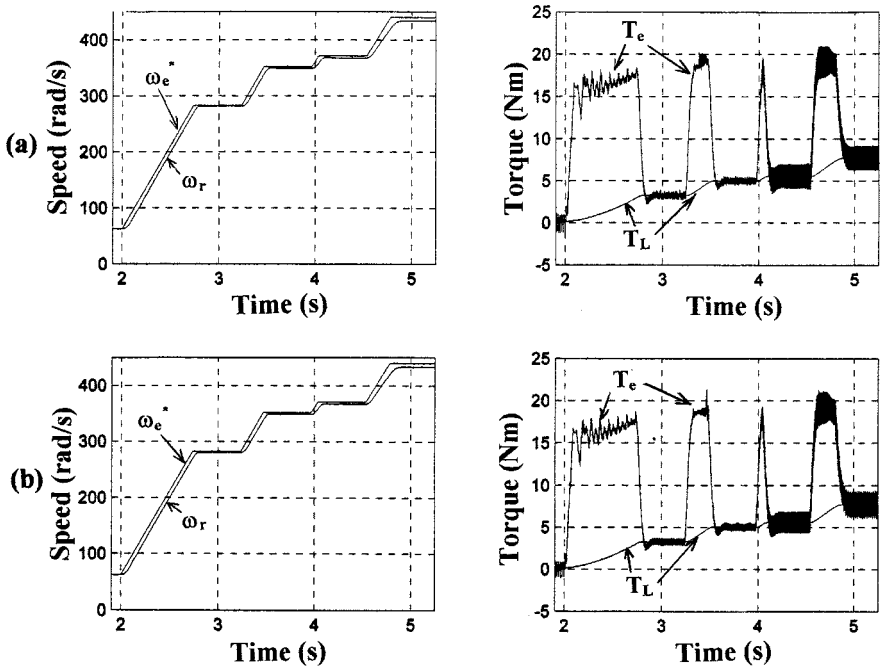

Fig. 10. V/Hz-controlled drive performance covering all the modes. (a) Neural-network-based SVM. (b) Conventional DSP-based SVM.

D. Simplification of Overmodulation Region

Solving the $T_{A-\mathrm{ON}}$ curves shown in Fig. 4 for undermodulation and overmodulation Mode-1 and Mode-2 by the respective equation sets for generating the neural network training data gives a considerable amount of complexity. It can be shown that the undermodulation curve can be expanded to Mode-1 and Mode-2 by using a nonlinear scale factor $f(V^*)$, as shown in Fig. 5, in order to get linear transfer characteristics in the whole range. The idea of this simplification is analogous to the sinusoidal PWM overmodulation principle where the modulating voltage is magnified. In the undermodulation region, $f(V^*) = V^*$, as explained before. This means that the $g(\alpha^*)$ curve can be plotted in Fig. 4 and multiplied by V^* to get $T_{A-\mathrm{ON}}$. In Mode-1, $f(V^*)$ is determined by using (13) and Fig. 3(a). In the proposed simplification, it can be shown that the curves are prone to some error only in sectors 2 and 3. Rigorous evaluation indicates that the average error is less than 0.28% by this simplification. For Mode-2 operation, the scale factor is determined by expanding the undermodulation curve and matching with the curve established by analysis. The resulting average error is below 0.5%. As shown in Fig. 5, $f(V)$ increases steeply in Mode-2 until it is theoretically infinity at square wave.

E. Neural Network—Angle and Amplitude Subnets

The derivation of turn-on time $T_{A-\mathrm{ON}}$ and simplification of modes discussed in the previous section permit ANN-based SVM implementation using two separate subnets: angle subnet and amplitude subnet. Fig. 6 shows the proposed ANN topology including the timer section. The subnets use a multilayer perception-type network with sigmoidal-type transfer function. The bias is not shown in the figure. The composite network uses two neurons at the input, 20 neurons in the hidden layer, and four output neurons. The input signal to the angle subnet is θ_e angle which is normalized and then pulsewidth functions at unit amplitude are solved (or mapped) at the output for the three phases, as indicated. The amplitude subnet implements the $f(V^*)$ function of Fig. 5. The digital words corresponding to turn-on time are generated by multiplying the angle subnet output with that of the amplitude subnet and then adding the $T_s/4$ bias signal, as shown. The PWM signals are then generated using a single timer. The angle subnet is trained with an angle interval of 2.16° in the range of 0°–360°. The backpropagation algorithm in the MATLAB Neural Network Toolbox is used for the training. The angle subnet takes 4800 epochs for training with an error below 0.5%. The amplitude subnet was trained with data at 1.0 V increments in the range of 0–191 V. It takes 1750 epochs for the training with an error below 1.0%. The training data size and the corresponding training time are, thus, reasonably small. It is important to note that, due to learning or interpolation capability, both the subnets will operate with higher signal resolution. Two values of sample time (T_s) are used in the project, i.e., 50 μs that corresponds to 20-kHz switching frequency and 100 μs that corresponds to 10-kHz switching frequency. The network is solved every sampling time to establish pulsewidth signals at the output. Note that the network works well in the full frequency range, including dc (zero frequency) condition.

IV. Performance Evaluation of Indirect Method

As mentioned before, the ANN-based SVM was implemented for the PWM controller and the drive system performance was evaluated. Once the network was trained and tested in the full range of voltage and frequency using sampling time $T_s = 100$ μs (10 kHz) and 50 μs (20

kHz), it was integrated with a V/Hz-controlled induction motor drive (Fig. 1). Table I shows the parameters of the drive system. The estimated computation time of the PWM controller is 40 μs with a TMS320C30-type DSP. Unfortunately, no suitable commercial ASIC chip is yet available [14] to implement the controller economically. The drive performance was evaluated in detail in undermodulation and overmodulation regions and compared with the performance of a conventional SVM-controlled drive. They were found to correlate very well. Fig. 7(a) shows the undermodulation phase current waves at 45-Hz frequency, and Fig. 7(b) shows the corresponding waves with the conventional DSP-based modulator. The distortion of both cases was analyzed by fast Fourier transform (FFT) and found to be 0.025% and 0.023%, respectively (note that a six-step wave has 4.5% distortion). The training algorithm simplification and finite training error of the ANN did not seem to contribute much performance deterioration. Fig. 8 shows the corresponding comparison of current waves in overmodulation Mode-1 at 56 Hz. Although the waveforms look practically identical, the distortion of the ANN-based SVM was 0.176%, and for the conventional SVM it was 0.091%. Fig. 9 shows the current waves in overmodulation Mode-2 at 59 Hz. The corresponding distortions were 0.858% and 0.278%. The drive was then accelerated in steps with ramp frequency command to cover operation in all the modes, and performance was found to be excellent. Fig. 10 shows the comparison of performance with fan load (see Table I) where speed ω_r is indicated in electrical radians per second. The drive goes into overmodulation region at 344 rad/s ($m = 0.907$) and field-weakening region at 377 rad/s ($m = 1$). The drive is accelerated with ramp speed command (ω_e^*) within the constraint of rated torque (20 N·m). The actual speed follows the command except the difference of positive slip frequency. Some amount of oscillatory behavior is evident in open-loop control, particularly at low speed. As the speed enters into the overmodulation and field-weakening regions, the ripple in the developed torque due to distortion in the current wave is evident. The ANN-based SVM with $T_s = 100$ μs was similarly evaluated in the drive and the performance correlated equally well. Currently, the PWM controller is being used successfully in a stator-flux-oriented vector-controlled induction motor drive.

V. Conclusion

A neural-network-based space-vector modulator has been described that operates very well in undermodulation as well as in overmodulation (Mode-1 and Mode-2) regions. The digital words corresponding to turn-on time are generated by the ANN and then converted to pulsewidths through a single timer. The scheme uses a backpropagation-type feedforward network. The training data and training time are reasonably small. The method can operate from dc (zero frequency). The scheme has been fully implemented and evaluated with a V/Hz-controlled induction motor drive, and gives excellent performance. The PWM controller is currently being used in a stator-flux-oriented vector-controlled induction motor drive. The ANN-based SVM can give higher switching frequency, which is not possible by conventional DSP-based SVM. The switching frequency can be easily extended up to 50 kHz if the ANN is implemented by a dedicated hardware ASIC chip.

References

[1] J. Holtz, "Pulse width modulation for electric power conversion," *Proc. IEEE*, vol. 82, pp. 1194–1214, Aug. 1994.

[2] J. O. Krah and J. Holtz, "High performance current regulation for low inductance servo motors," in *Conf. Rec. IEEE-IAS Annu. Meeting*, 1998, pp. 490–499.

[3] B. K. Bose, *Power Electronics and AC Drives*. Englewood Cliffs, NJ: Prentice-Hall, 1986.

[4] F. Harashima *et al.*, "Applications of neural networks to power converter control," in *Conf. Rec. IEEE-IAS Annu. Meeting*, 1989, pp. 1086–1091.

[5] M. R. Buhl and R. D. Lorenz, "Design and implementation of neural networks for digital current regulation of inverter drives," in *Conf. Rec. IEEE-IAS Annu. Meeting*, 1991, pp. 415–423.

[6] J. W. Song, K. C. Lee, K. B. Cho, and J. S. Won, "An adaptive learning current controller for field-oriented controlled induction motor by neural network," in *Proc. IEEE IECON'91*, 1991, pp. 469–474.

[7] M. P. Kazmierkowski, D. L. Sobczuk, and M. A. Dzieniakowski, "Neural network current control of VS-PWM inverters," in *Proc. EPE'95*, 1995, pp. 1415–1420.

[8] A. Bakhshai, J. Espinoza, G. Joos, and H. Jin, "A combined artificial neural network and DSP approach to the implementation of space vector modulation techniques," in *Conf. Rec. IEEE-IAS Annu. Meeting*, 1996, pp. 934–940.

[9] H. W. Van Der Broeck, H. C. Skudelny, and G. Stanke, "Analysis and realization of a pulse width modulator based on voltage space vectors," *IEEE Trans. Ind. Applicat.*, vol. 24, pp. 142–150, Jan./Feb. 1988.

[10] J. Holtz, W. Lotzkat, and M. Khambadkone, "On continuous control of PWM inverters in the overmodulation range including the six-step mode," *IEEE Trans. Power Electron.*, vol. 8, pp. 546–553, Oct. 1993.

[11] S. Bolognani and M. Ziglitti, "Novel digital continuous control of SVM inverters in the overmodulation range," *IEEE Trans. Ind. Applicat.*, vol. 33, pp. 525–530, Mar./Apr. 1997.

[12] J. Kim and S. Sul, "A novel voltage modulation technique of the space vector PWM," in *Proc. Int. Power Electronics*, Yokohama, Japan, Apr. 1995, pp. 742–747.

[13] D. C. Lee and G. M. Lee, "A novel overmodulation technique for space vector PWM inverters," *IEEE Trans. Power Electron.*, vol. 13, pp. 1144–1151, Nov. 1998.

[14] L. M. Reynery, "Neuro-fuzzy hardware: design, development and performance," in *Proc. IEEE-FEPPCON III*, Kruger National Ppark, South Africa, July 1998, pp. 233–241.

[15] B. K. Bose, Ed., *Power Electronics and Variable Frequency Drives*. Piscataway, NJ: IEEE Press, 1997.

Joao O. P. Pinto (S'97) received the B.S. degree from the Universidade Estadual Paulista, Ilha Solteira, Brazil, and the M.S. degree from the Universidade Federal de Uberlândia, Uberlândia, Brazil, in 1990 and 1993, respectively. He is currently working toward the Ph.D. degree at the University of Tennessee, Knoxville.

He has been an Assistant Professor at the Universidade Federal do Mato Grosso do Sul, Campo Grande, Brazil, since 1994. His research interests include neural networks, fuzzy logic, genetic algorithms, and wavelet applications to power electronics, PWM techniques, drives, and machine control.

Bimal K. Bose (S'59–M'60–SM'78–F'89–LF'96) received the B.E. degree from Calcutta University (Bengal Engineering College), Calcutta, India, the M.S. degree from the University of Wisconsin, Madison, and the Ph.D. degree from Calcutta University in 1956, 1960, and 1966, respectively.

He currently holds the Condra Chair of Excellence in Power Electronics at the University of Tennessee, Knoxville, where he has been responsible for organizing the power electronics program for the last 13 years. He is also the Distinguished Scientist (formerly Chief Scientist) of the EPRI-Power Electronics Applications Center, Knoxville, TN, Honorary Professor of Shanghai University, China University of Mining and Technology, and Xian Mining Institute (also Honorary Director of the Electrical Engineering Institute), China, and Senior Adviser of the Beijing Power Electronics Research and Development Center, Beijing, China. Early in his career, he served as a Faculty Member at Calcutta University for 11 years. In 1971, he joined Rensselaer Polytechnic Institute, Troy, NY, as an Associate Professor of Electrical Engineering. In 1976, he joined General Electric Corporate Research and Development, Schenectady, NY, as Research Engineer and served there for 11 years. He has been a Consultant to more than ten industries. His research interests spread over the whole spectrum of power electronics, and specifically include power converters, ac drives, microcomputer control, EV drives, and expert system, fuzzy logic, and neural-network-based control of power electronics and drive systems. He has authored more than 150 published papers and is the holder of 21 U.S. patents. He is the author/editor of five books: *Power Electronics and AC Drives* (Englewood Cliffs, NJ: Prentice–Hall, 1986), *Adjustable Speed AC Drive Systems* (New York: IEEE Press, 1981), *Microcomputer Control of Power Electronics and Drives* (New York: IEEE Press, 1987), *Modern Power Electronics* (New York: IEEE Press, 1992), and *Power Electronics and Variable Frequency Drives* (Piscataway, NJ: IEEE Press, 1997). Another book, *Modern Power Electronics and AC Drives*, is to be published by Prentice-Hall. The book *Power Electronics and AC Drives* has been translated into Japanese, Chinese, and Korean.

Dr. Bose was the Guest Editor of the PROCEEDINGS OF THE IEEE Special Issue on Power Electronics and Motion Control (August 1994). He has received the GE Publication Award, Silver Patent Medal, and a number of IEEE Prize Paper Awards. He is listed in *Marquis' Who's Who in America*. He has served the IEEE in various capacities, including Chairman of the IEEE Industrial Electronics Society (IES) Power Electronics Council, Associate Editor of IEEE TRANSACTIONS ON INDUSTRIAL ELECTRONICS, IEEE-IECON Power Electronics Chairman, Chairman of the IEEE Industry Applications Society (IAS) Industrial Power Converter Committee, IAS member in the Neural Networks Council, and various other national and international professional committees. He has been a member of the Editorial Board of the PROCEEDINGS OF THE IEEE since 1995 and has served a large number of national and international conferences. He has served as a Distinguished Lecturer in the IAS and IES. For his research contributions, he was awarded the Premchand Roychand Scholarship and the Mouat Gold Medal by Calcutta University in 1968 and 1970, respectively. He received the IAS Outstanding Achievement Award in 1993, the IES Eugene Mittelmann Award in 1994, IEEE Region 3 Outstanding Engineer Award in 1994, IEEE Lamme Gold Medal in 1996, IEEE Continuing Education Award in 1997, and IEEE Millenium Medal in 2000.

Luiz Eduardo Borges da Silva (S'84–M'89) was born in Passa Quatro, Brazil. He received the B.S. degree in electrical engineering and the M.S. degree from the Escola Federal de Engenharia de Itajubá, Itajubá, Brazil, and the Ph.D. degree in power electronics from the Ecole Polytechnique de Montreal, Montreal, PQ, Canada, in 1977, 1982, and 1988, respectively.

From 1988 to 1992, he was the Head of the Electronics Department, Escola Federal de Engenharia de Itajubá. During 1998, he held a post-doctoral position in the Department of Electrical Engineering, University of Tennessee, Knoxville. He teaches power electronics and digital control systems at the Escola Federal de Engenharia de Itajubá, where he also works with the Power Electronics group. He is currently on leave at the University of Tennessee, Knoxville. His main research interests are applications of artificial intelligence in power electronics and signal processing.

Marian P. Kazmierkowski (M'89–SM'91–F'98) received the M.Sc., Ph.D., and Dr. Sc. degrees in electrical engineering from the Institute of Control and Industrial Electronics, Warsaw University of Technology, Warsaw, Poland, in 1968, 1972 and 1981, respectively.

From 1967 to 1969, he was with the Industrial Research Institute of Electrotechnics, Warsaw, Poland, and from 1969 to 1980, he was with the Institute of Control and Industrial Electronics, Warsaw University of Technology, as an Assistant Professor. From 1980 to 1983, he was with RWTH Aachen, Aachen, West Germany, as an Alexander von Humboldt Fellow. During 1986–1987, he was a Visiting Professor at NTH Trondheim, Trondheim, Norway. Since 1987, he has been a Professor and Director of the Institute of Control and Industrial Electronics, Warsaw University of Technology. He was a Visiting Professor at the University of Minnesota, Minneapolis, in 1990, at Aalborg University, Aalborg East, Denmark, in 1990 and 1995, and at the University of Padova, Padova, Italy, in 1993. He is also currently a Coordinating Professor in the International Danfoss Professor Program 1997–2000, Aalborg University. Since 1996, he has served as an elected member of the State Committee for Scientific Research in Poland. He is engaged in research and theoretical work on electrical drive control and industrial electronics. He is the author or coauthor of more than 140 technical papers and reports, as well as 11 books and textbooks. His latest book, with Dr. H. Tunia, is *Automatic Control of Converter-Fed Drives* (Amsterdam, The Nederlands: Elsevier, 1994).

Dr. Kazmierkowski was Chairman of the 1996 IEEE International Symposium on Industrial Electronics held in Warsaw, Poland. He is an Associate Editor of the IEEE TRANSACTIONS ON INDUSTRIAL ELECTRONICS, a Vice President of the IEEE Industrial Electronics Society, and the IEEE Industrial Electronics and IEEE Power Electronics Societies Joint Chapter Chairman of the Poland Section of the IEEE.